Available online at www.sciencedirect.com
ScienceDirect
Journal of Power Sources 172 (2007) 308–323
JOURNAL OF POWER SOURCES
www.elsevier.com/locate/jpowsour

Novel solid oxide fuel cell system controller for rapid load following

Fabian Mueller, Faryar Jabbari, Robert Gaynor, Jacob Brouwer*

National Fuel Cell Research Center, University of California at Irvine, Irvine, CA, United States

Received 16 April 2007; received in revised form 22 May 2007; accepted 22 May 2007
Available online 17 July 2007

Abstract

A novel SOFC system control strategy has been developed for rapid load following. The strategy was motivated from the performance of a baseline control strategy developed from control concepts in the literature. The basis for the fuel cell system control concepts are explained by a simplified order of magnitude time scale analysis. The control concepts are then investigated in a detailed quasi-two-dimensional integrated dynamic system model that resolves the physics of heat transfer, chemical kinetics, mass convection and electrochemistry within the system.

The baseline control strategy is based on the standard operating method of constant utilization with no control of the combustor temperature. Simulation indicates that with this control strategy large combustor transients can take place during load transients because the fuel flow to the combustor increases faster than the air flow. To alleviate this problem, a novel control structure that maintains the combustor temperature within acceptable ranges without any supplementary hardware was introduced. The combustor temperature is controlled by manipulating the current to change the combustor inlet stoichiometry. The load following capability of SOFC systems is inherently limited by anode compartment fuel depletion during the time of fuel delivery delay. This research indicates that future SOFC systems with proper system and control configurations can exhibit excellent load following characteristics.

Keywords: SOFC; Decentralized controller; System control; Dynamic simulation; Time scale analysis

1. Introduction

The goal of this paper is to (1) identify and analyze challenges of load following in solid oxide fuel cells, (2) design a system configuration and control strategy for rapid system load following, and (3) discuss inherent load following limitations for particular control architecture. In simple cycle solid oxide fuel cell (SOFC) systems, all the power is generated by the fuel cell. A reformer, combustor and blower are needed to support the operation of the SOFC. To meet the power demand the SOFC must generate power to meet both the external power demand and the parasitic (or internal) power of the balance of plant. SOFC system electrical power is generated from the electrochemical potential between fuel at one electrode–electrolyte interface and air at an opposing electrode–electrolyte interface. SOFC electrochemical reaction rates are quite rapid, typically occurring over time periods on the order of milliseconds [1]. Since the electrochemistry directly produces the electrical work output, SOFC technology should be able to achieve rapid load following capability on the same order as that offered by the electrochemistry. Load following problems occur when the response of the fuel cell system cannot safely meet both the external system power demand and the balance of plant power demand. The limitations could result from conservative control techniques or from inherently slow response of subsystem components, such as flow or chemical reaction delays associated with fuel processing equipment. In the case of slow subsystem response the fuel cell performance must be slaved to the performance of the subsystem.

A control system is needed to interconnect each of the system components and to meet the power demand within the operating requirements of the system. Different control strategies can be implemented with different performance. In this paper, two different control strategies are presented. The first control strategy is based on control concepts found in the literature with some slight control improvements. The control concepts are investigated in detail, with special attention to overall challenges and limitations. Based on the control transients, and insight into control limitations, a new control architecture is

* Corresponding author. Tel.: +1 949 824 1999; fax: +1 949 824 7423.
E-mail addresses: fm@nfcrc.uci.edu (F. Mueller), fjabbari@uci.edu (F. Jabbari), rmg@nfcrc.uci.edu (R. Gaynor), jb@nfcrc.uci.edu (J. Brouwer).

0378-7753/$ – see front matter © 2007 Elsevier B.V. All rights reserved.
doi:10.1016/j.jpowsour.2007.05.092

Nomenclature

C	solid specific heat capacity (kJ kg^{-1} K^{-1})
C_V	constant volume gas specific heat capacity (kJ kmol^{-1} K^{-1})
F	Faradays constant (96,487 C mol^{-1})
h	enthalpy (kJ kmol^{-1})
h_f	enthalpy of formation (kJ kmol^{-1})
i	current (A)
J	moment of inertia (kg m^2)
k_{cell}	number of cells in stack
k_{ref}	number of reformers in system
m	mass (kg)
N	molar capacity (kmol)
$\dot{N}$	molar flow rate (kmol s^{-1})
P	pressure (kPa)
$\dot{Q}$	heat transfer (kW)
$\dot{R}$	species reaction rate (kmol s^{-1})
R	universal gas constant (8.3145 J mol^{-1} K^{-1})
t	time (s)
T	temperature (K)
U	utilization
V	volume (m^3)
w	rotational velocity (rad s^{-1})
$\dot{W}$	rate of work (kW)
X	species mole fraction

Greek letters

γ	ratio of specific heats
η	efficiency
ρ	density of solid (kg m^{-2})

Control variables

b	feedback contribution
d	demand value
e	error between feedback and set point value
f	feed forward contribution
g	modified or governed signal
N_{fc}	fuel flow rate (kmol s^{-1})
P	external power demand (kW)
P_{fc}	Fuel cell power (kW)
PB	blower power (kW)
r	reference set point value
RPM	blower shaft speed (rpm)
t_c	combustor temperature (K)
T_{stack}	fuel cell stack temperature (K)
u	system input
y	system feedback value

developed. Improvements provided by this control strategy are demonstrated and explained.

The key to demonstrating control concepts is to analyze the system transient response in comparison to the system operating requirement. Ideally, an experimental system could be used, however due to the cost and unavailability of such a system, the transient response of a SOFC system was investigated through dynamic modeling and simulation of an integrated system. The model is nonlinear based on transport and conservation principles. The modeling methodology used has been verified experimentally and utilized for controls development in previous work [2–9]. Since the focus of the paper is controls, the physical dynamic model is only briefly presented in Appendix A.

2. Background

The challenge during load following is to safely operate the system within known operating requirements and constraints. General fuel cell system operating requirements as expressed in the literature are:

(1) The steam-to-carbon ratio in the fuel cell fuel supply must be greater than two to avoid carbon coking in the fuel lines, reformer, and fuel cell stack [6,10–12].
(2) Electrochemically active fuel species (mainly hydrogen) cannot be depleted in the fuel cell [6,10,13]. Sufficient fuel and oxidant is required to support the electrochemical reactions and must always be supplied to avoid electrode redox. Preferably the fuel utilization remains less than 95% to incorporate a margin of safety.
(3) Thermal stresses should be avoided throughout the system to maximize material durability and lifetime.
   a. Fuel and air temperatures at the entrance to the fuel cell stack should be maintained to within 200 K of the fuel cell operating temperature [6,7,10,14,15].
   b. Endothermic cooling caused by fuel reformation reactions at the fuel cell anode inlet should be minimized. The fuel is usually pre-reformed before entering the fuel cell anode compartment [10,15,16].
   c. Combustor and heat exchanger temperature extremes and thermal transients should be minimized [11,17,18].
(4) Fuel cell degradation must be avoided.
   a. The fuel cell operating temperature should be maintained as close as possible to the design temperature (∼10 K) to avoid thermal fatigue [10,11,14].
   b. The fuel cell voltage should be maintained at all times to avoid high local heat production rates [10,16].

When operating a SOFC system, the above set of operating requirements must be satisfied at all times including during transient operation. The fuel cell stack requirements are the most stringent of any component in the system, but operating requirements of other major components and the entire balance of plant must correspondingly be satisfied at all times.

A reasonable amount of controls research for SOFC systems has been presented in the literature to ensure that these SOFC operating requirements can be satisfied. Most research groups have investigated overall system controls [4,6,8,10,11,13] while some have investigated specific operating requirements in more detail [5,7,14,19]. While the control strategies developed vary to some extent, a seemingly effective control strategy to meet system power demand and maintain the fuel cell operating

requirements suggested by the literature includes the following features:

(1) Manipulate current to follow the system power demand [6,8,10,19].
(2) Manipulate fuel flow to maintain fuel utilization (operating requirement 2) [5,6,10,13,19].
(3) Provide water from an external source or re-circulate sufficient anode depleted fuel to maintain a high steam-to-carbon ratio (operating requirement 1) [6,10].
(4) Design and manipulate the SOFC balance of plant to maintain the fuel cell inlet temperature (operating requirement 3a) [6,7,10,14].
(5) Manipulate the cathode airflow rate to maintain the fuel cell temperature (operating requirement 4a) [6–8,10,13,14].
(6) Limit the amount of current drawn to assure that electrochemically active fuel species are not depleted in the fuel cell and that the fuel cell voltage remains at reasonable values (operating requirements 2 and 4b) [6,8,10,19].

The baseline control design used here initially is based on these six basic control concepts. Development and analysis of the controller is presented. While the baseline control strategy is effective and can be designed for significant load following capability, the baseline controller does not sufficiently control the combustor temperature for rapid load following cases. Dynamic simulation results indicate thermal transients in the combustor are a cause of concern when the baseline controller is used. A novel alternative control strategy is proposed to address the limitations of baseline control design regarding control of combustor temperature.

3. System

While this paper attempts to investigate SOFC systems and controls broadly, a specific system is required to demonstrate and investigate control designs of the concepts developed. To meet this need, an integrated dynamic model of the 5 kW simple cycle system, presented in Fig. 1, was developed. The system is a typical simple cycle SOFC system in the 5 kW scale with key design features that are included for load following capability.

In this system, a variable speed blower is used, such that the air flow can be controlled to maintain the fuel cell temperature at

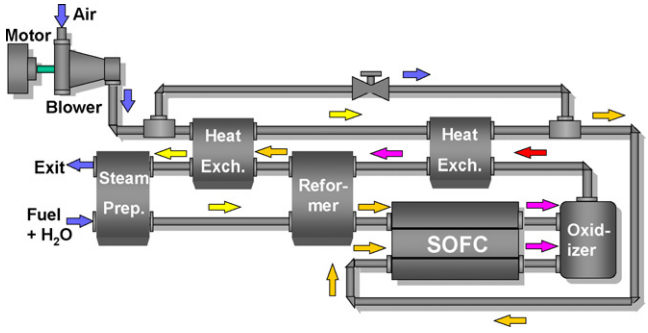

Fig. 1. Schematic of the nominal 5 kW integrated SOFC system.

1150 K (control concept 5). The air is preheated using the combustor exhaust. Two air-exhaust heat exchangers are utilized; a high temperature (ceramic) heat exchanger and a stainless steel heat exchanger. Typical stainless steel heat exchangers should be maintained below 930 K but ceramic heat exchangers can handle temperatures up to 1400 K [18] depending upon material type and design. Use of a high temperature heat exchanger is required in the current system because of high combustor temperatures and the fuel cell requirement of high inlet air temperature (1000 K). Cold air can bypass the heat exchangers. This allows for effective control of the cathode inlet temperature (control concept 4).

Water required for fuel reformation is supplied to the system from an external source (control concept 3). A steam preparation boiler is used to vaporize liquid water to steam using the system exhaust. To minimize thermal gradients in the fuel cell (operating requirement 3b), the natural gas-steam stream is reformed prior to supply to the fuel cell anode compartment. The heat required by the reformation is supplied by the system combustor exhaust. In the current system configuration, it was found beneficial to use the exhaust to heat the reformer using a stainless steal heat exchanger placed between the two high temperature heat exchangers to ensure a sufficient temperature in the reformer. In the current configuration the reformer temperature is sufficient to ensure more than 90% methane conversion to hydrogen and carbon monoxide in the reformer.

The system is analyzed using a dynamic model. A summary of the system dynamic model is presented in Appendix A. The model is based on the physics and chemistry that govern the fuel cell system, and is developed by resolving conservation of mass, energy, and momentum principles, with corresponding electrochemistry, chemical kinetics, heat generation, and heat transfer. While the specific configuration used here has not been verified experimentally, the model for different subsystems has been verified experimentally with other configurations, and the current approach has been used previously to investigate fuel cell system control design [2–9].

4. Baseline design

It is known that the electrochemical time scale of fuel cells is very rapid, on the order of microseconds [1]. Power electronic response times are similarly fast. Because of the fast electrochemical response time in a SOFC, system load demands can be met rapidly by manipulating the current using modern power electronics [6,8,10,19].

If (a) hydrogen supply was unlimited, (b) thermal constraints were not an issue, and (c) steam supply was certain, then SOFC systems should have very rapid load following capability. SOFC system dynamic response could be on the order of timescales associated with system control strategies (e.g., milliseconds), not exceeding those associated with electrochemistry and power electronics. This would be the ideal case for a SOFC system. However, a multitude of challenges and constraints (to SOFC system transient load following capabilities) are imposed by requirements of long-term reliability (which demands strict control of thermal gradients and transients), and interactions

caused by slower system component response times (reformer flow response, and blower shaft dynamics), as discussed further below.

4.1. Fuel depletion

Following a load increase in the fuel cell, all electrochemically active species in the anode compartment will begin to be consumed in the fuel cell at a higher rate. In the current analyses hydrogen (the most important electrochemically active species) is assumed to be the only electrochemically active species. The water gas shift and steam reformation reactions are resolved such that carbon monoxide and methane will be converted to hydrogen as hydrogen is consumed. Full system model simulation indicates that for a large load increases the active species within the fuel cell anode compartment will become depleted in fractions of a second if new additional fuel is not supplied. As an order magnitude time scale check, the time scale of hydrogen depletion within the fuel cell can be characterized generally from mass conservation as:

$$O(\Delta t) = -\frac{UnFN}{i_1} \ln\left(\frac{(i_2/i_1)U + X_{\min} - 1}{(i_2/i_1)U - U}\right) \quad (1)$$

From constants for the system listed in Table 1, the order of magnitude check results in approximately half a second for hydrogen depletion consistent with model prediction. From system operating requirement 2, fuel must be maintained within the fuel cell at all times. The rate of hydrogen consumption within each fuel cell is directly proportional to the current

$$\mathrm{H_2\ consumed} = \frac{i}{2F} \quad (2)$$

Therefore, when current is increased, hydrogen consumption within the fuel cell is increased. Since it is known that hydrogen or fuel consumption is proportional to the current, it is possible to control the system inlet fuel flow rate in direct proportion to the current so as to maintain constant fuel utilization as follows:

$$\dot{N}_{\mathrm{in}} = \frac{ik_{\mathrm{cell}}}{U2FX_{\mathrm{H_2}} \times 1000} \quad (3)$$

where U represents the operating utilization, $X_{\mathrm{H_2}}$ the inlet fuel potential hydrogen content, and k_{cell} is the number of cells in the SOFC stack. This is a popular fuel flow control strategy in literature [5,8,19] called current-based fuel control. If hydrogen could be instantaneously supplied to the fuel cell using current-based fuel control, and thermal restrictions did not apply, then SOFC systems could exhibit transient load following capabilities that are only constrained by the time scale of the electrochemistry.

Table 1
Values used in time analysis

i_1 (A)	20	Initial current
i_2 (A)	70	Final current
V_1 (V)	0.8	Initial voltage
V_2 (V)	0.67	Final voltage
R (Ω)	0.0046	Internal resistance
P (kPA)	101.325	Operating pressure
U (%)	85	Steady state operating utilization
$X_{\min}$ (%)	5	Minimum fuel cell hydrogen mole percent
ΔT (K)	10	Temperature increase
T (K)	1150	Fuel cell temperature
T_{ref} (K)	955	Reformer temperature
$\Delta \dot{W}_{\mathrm{blower}}$ (W)	200	Blower power increase during transient

In practical systems, the flow of hydrogen to the fuel cell cannot increase instantaneously because of delays in fuel delivery, preparation, and processing. This delay can include flow delays in valve actuation, flow delay in the fuel desulfurizers, delays caused by the reformer chemical kinetics including those from insufficient heat transfer to the reformer and insufficient reformer residence time, as well as reformer mass flow delays. The model considered in this paper resolves the reformer in a quasi-two-dimensional manner, capturing the chemical kinetics of steam reformation (implementing the kinetics models from [20,21]), the heat transfer from the exhaust stream to the reformate stream required to balance the endothermic steam reformation reaction, as well as the reformer mass flow delay due to pressure transients in the reformer as explained in [22,23]. Note that flow delays associated with actuators and the desulfurizer are not physically resolved but are essentially lumped into the reformer mass flow delay.

Fuel flow delays are cause for concern because for sufficiently large load increases, hydrogen can become depleted in the fuel cell before the reformer exit fuel flow is sufficiently increased. In the ideal case that the reformer exit stream composition can be maintained during transients, the mass flow response of the reformer can still limit or affect the dynamic system performance. The reformer exit flow does not increase instantaneously with an increase in reformer inlet flow due to flow restrictions between the reformer and anode. The pressure gradient across the flow restriction must increase before the flow into the reformer increases. The mass flow delay due to pressure effects in the reformer volume alone can be longer than the time for the hydrogen within the fuel cell to become depleted. From mass conservation

$$\frac{\mathrm{d}N}{\mathrm{d}t} = \dot{N}_{\mathrm{in}} - N_{\mathrm{out}} + \sum \dot{R} \quad (4)$$

And the orifice flow equation

$$\dot{N}_{\mathrm{out,ss},j} = \dot{N}_{\mathrm{o}} \sqrt{\frac{P_{\mathrm{in}} - P_{\mathrm{out},j}}{\Delta P_{\mathrm{o}}}} \quad (5)$$

By assuming current based fuel control, 100% methane conversion, a steam to carbon ratio of 2, and ideal gas, the order of magnitude first approximation for the fuel flow rate at the reformer exit increase to steady state can be estimated as:

$$O(\Delta t) = \frac{V}{RT}\frac{5}{3}\frac{k_{\mathrm{cell}}}{k_{\mathrm{ref}}}\frac{3}{4}\frac{1}{UnF}\frac{\Delta P_{\mathrm{o}}}{\dot{N}_{\mathrm{o}}^2}(i_2 - i_1) \quad (6)$$

From constants for the system listed in Table 1, considering a 20–70 A instantaneous load increase in the present system, the order of magnitude check results in approximately 3 s for the reformer fuel flow rate to increase to steady state values. Considering only the mass flow delay in the reformer, 3 s for the fuel cell–fuel flow to increase, is long enough for fuel to

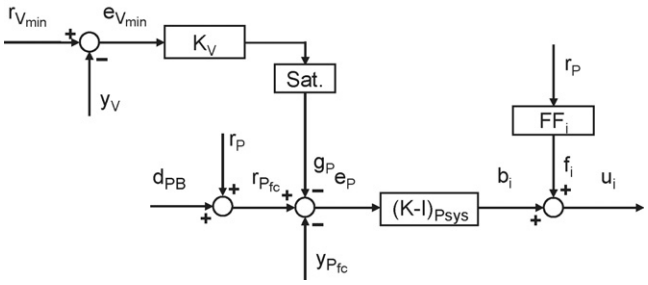

Fig. 2. Fuel cell power controller with reference governor (*y* indicates system feedback value, *r* indicates reference set point value, *e* indicates error between feedback and set point value, *g* indicates modified/governor contribution, *u* indicates system input value, *f* indicates feed-forward contribution, *b* indicates feedback contribution, *d* indicates demand value).

become depleted in the fuel cell. The order of magnitude time analysis illustrates the problem of fuel cell–fuel depletion during reformer flow delays.

Since it is necessary that sufficient hydrogen remain in the fuel cell, the current drawn from the fuel cell during load increases should be limited (governed) by the available rate of hydrogen supply. This is particularly true during the time of the reformer flow delay that can occur during large load transients.

To ensure that electrochemically active fuel is not depleted in the fuel cell, voltage measurement can be used to indicate depleting species within the fuel cell. Specifically, the fuel cell voltage is strongly dependent on hydrogen concentration. The dependence of voltage on hydrogen concentration in the anode compartment is classically evaluated from the Nernst equation. In particular, since fuel cell voltage rapidly adjusts to the limiting local species concentrations in the cell, the voltage can be measured in real time, providing rapid, robust, and cost effective information on electrochemically active species within the fuel cell. Deducing hydrogen concentration in the anode compartment via monitoring voltage is consistent with hydrogen sensors that have been developed based on the electrochemical potential of hydrogen [24–28]. To avoid hydrogen depletion within the fuel cell, the fuel cell power can be governed as illustrated in Fig. 2 by limiting the fuel cell power demand whenever low voltage operating conditions are observed. Thus, fuel cell power demand is constrained whenever hydrogen becomes depleted in the fuel cell anode compartment.

Under normal operating conditions the fuel cell power demand (system output power demand plus parasitic power, labeled blower power, demand) is controlled by manipulating the fuel cell current using the feedback and feed-forward controller, as shown in Fig. 2. When the fuel cell voltage (y_V) becomes less than a minimum set value ($r_{V_{min}}$) the fuel cell power demand ($r_{P_{fc}}$) is lowered to a modified power demand (g_p). The fuel cell power ($y_{P_{fc}}$) is then controlled to the modified power demand (g_P) by manipulating the current drawn from the fuel cell (u_i). Constants for each controller are presented in Table 2. Current feed-forward is based on the reference system power demand. A steady state current versus reference power look-up table is used to determine the feed-forward current (f_i) from the reference power demand. All of the feed-forward control logic in this paper is based on system steady state operation look-up tables. Since the response of electrochemistry is fast (assumed instantaneous in the model) large feedback gains can be used in a stable fashion to control the system power.

This control strategy will prevent the fuel cell voltage from dropping below a minimum value; ensuring that the active species in the fuel cell anode compartment will not be depleted. If the active species becomes depleted then the fuel cell chemical potential becomes zero, and the corresponding fuel cell voltage becomes zero. While still connected to a load that draws current, anode materials may be oxidized (to consume oxygen ions and produce electrons) in the place of fuel. This can be followed by reduction once fuel is returned to the interface, but, repeated redox of this type can severely damage a fuel cell anode. A sufficiently large gain (K_v) must be used so that the power will effectively control the voltage to prevent anode redox.

Table 2
Controller constants

Power controller with reference governor		
$K_{P_{sys}}$ ($A\,kW^{-1}$)	50	System power feedback proportional gain
$I_{P_{sys}}$ ($A\,kW^{-1}$)	5	System power feedback integral gain
$r_{V_{min}}$ (V)	0.65	Cell minimum voltage
K_V ($kW\,V^{-1}$)	100	Fuel cell power reference governor gain
Sat (kW)	>0	Power reference governor saturation
Blower cascade controller		
$r_{T_{stack}}$ (K)	1150	Reference fuel cell operating temperature
$K_{T_{stack}}$ ($rpm\,K^{-1}$)	300	Temperature feedback proportional gain
K_{RPM} ($\times 10^{-3}\,kW\,rpm^{-1}$)	2	Shaft speed feedback proportional gain
Sat (kW)	0.015–0.5	Blower power saturation
Fuel cell current combustor temperature controller		
K_{tc} ($A\,k^{-1}$)	1.2	Combustor temperature feedback gain
Rate ($K\,s^{-1}$)	±0.02	Combustor temperature set point ramp rate
Sat (A)	10–85	Current saturation
Fuel flow fuel cell power controller		
$K_{P_{fc}}$ ($\times 10^{-6}\,kmol\,kW^{-1}$)	3.5	Fuel cell power feedback proportional gain
$I_{P_{fc}}$ ($\times 10^{-9}\,kmol\,kW^{-1}$)	1	Fuel cell power feedback integral gain

When a power reference governor is implemented to avoid hydrogen depletion, the fuel cell fuel flow cannot be controlled solely using current-based fuel control. This is because when the fuel cell current is limited due to low fuel cell hydrogen concentration the system inlet fuel flow is automatically lowered if only current-based fuel control is used. This is problematic since the current was reduced due to insufficient fuel being sent to the fuel cell anode compartment. To avoid this challenge the system inlet flow rate is set to the larger of the two flow rates as determined by (1) current-based fuel control and (2) feed-forward fuel flow based on the fuel cell power demand. It could be possible to operate the controller with only the feed-forward controller, but implementing current-based fuel control is a practical strategy for dealing with errors in the feed-forward look up table, system degradation, or other system performance changes.

4.2. Fuel cell thermal management

The temperature of the fuel cell stack must be closely maintained during transient operation. As the current is increased both the power and heat generated within the fuel cell increase, which within a typical operating envelope follow a linear proportionality that relates current to voltage through the Ohmic resistance. Research has been indicating that variable speed actuation of air is beneficial for effectively controlling temperatures in SOFC systems [6–8,10,13,14].

Manipulating the air flow to control the fuel cell temperature is effective because the thermal response time of the fuel cell stack is larger then the time scale of air actuation. On an order of magnitude time scale analysis, the thermal response time can be approximated with out considering convective cooling from the air as:

$$O(\Delta t) = \frac{mC\Delta T}{\dot{Q}_{\text{in}}} = \frac{\Delta T(m_{\text{mea}}C_{\text{mea}} + m_{\text{gas}}C_V + m_{\text{p}}C_p)\Delta T}{(\Delta i/nF)h_{\text{f}} - \Delta(iV)} \tag{7}$$

And the blower response time can be approximated on an order of magnitude scale as:

$$O(\Delta t) = \frac{((\dot{m}_2/\beta\,\text{mm})^2 - (\dot{m}_1/\beta\,\text{mm})^2)}{2}\frac{J}{\Delta\dot{W}_{\text{blower}}} \tag{8}$$

where the initial and final mass flow rate to maintain the fuel cell air between inlet and outlet temperature (T_{in} and T_{out}) can be evaluated from an energy balance as

$$\dot{m}_i = k\frac{(i_i/nF)h_{\text{f}} - (iV)_i}{h_{\text{out}}(T_{\text{out}}) - h_{\text{in}}(T_{\text{in}})} \tag{9}$$

For a large power increase for system values presented in Table 1, the fuel cell thermal time scale is on the order of 217 s and the blower air response time is on the order of 3 s indicating the blower response is significantly faster than the fuel cell thermal response time.

The time scale in which the air flow can be manipulated depends upon the blower moment of inertia and the amount of power used by the blower. Therefore, the time scale of the blower can be controlled to meet the thermal operating requirement of the fuel cell. Even for small blower power, the time scale associated with increasing air flow is significantly smaller than the stack thermal time scale. This indicates the air can effectively be manipulated to control the fuel cell temperature.

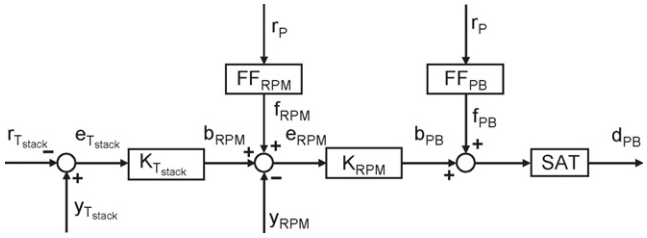

Fig. 3. Blower cascade controller (y indicates system feedback value, r indicates reference set point value, e indicates error between feedback and set point value, g indicates modified/governor contribution, u indicates system input value, f indicates feed-forward contribution, b indicates feedback contribution, d indicates demand value).

To increase the air flow rate, following a load change, a cascade blower controller is utilized as shown in Fig. 3. The fuel cell stack temperature ($y_{T_{\text{stack}}}$) is controlled by manipulating the blower shaft speed feedback (b_{RPM}). The blower shaft speed (y_{RPM}) is then controlled by demanding more blower power (b_{PB}). To control both the fuel cell stack temperature and blower shaft speed as quickly as possible, a feed-forward, and feedback control is used in each. Feed-forward control is required because the response time of the fuel cell stack temperature is large and because only small variations in fuel cell temperature occur in the immediate aftermath of dynamic load variations. If feed-forward control were not used thermal "runaway" might occur. Constant values used in the cascade fuel cell temperature and blower shaft speed controller are presented in Table 2.

In order to meet both the external and blower power demand the fuel cell power demand set point ($r_{P_{\text{fc}}}$) is set equal to the system power demand (r_{p}) plus the blower power demand (d_{PB}).

$$r_{P_{\text{fc}}} = r_{\text{p}} + d_{\text{PB}} \tag{10}$$

In order to limit the impact of the blower power demand on load following, the blower power demanded from the fuel cell is not the actual power sent to the blower. Instead, the actual blower power (u_{PB}) is taken to be the actual fuel cell power ($y_{P_{\text{fc}}}$) minus the load power demand (r_{p}) with the blower power constrained to be positive

$$u_{\text{PB}} = y_{P_{\text{fc}}} - r_{\text{p}} \tag{11}$$

In this way, the system power output (y_{p}) will be equal to the power demand, unless the blower power (u_{PB}) becomes zero

$$y_{\text{p}} = y_{P_{\text{fc}}} - u_{\text{PB}} \tag{12}$$

Once the fuel cell power set point is tracked (due to integral feedback) the blower power demand will be the actual blower power. This approach forces the blower power to be manipulated as quickly as possible, but limited to values that do not negatively affect the system power response. By controlling the blower power and fuel cell power in this fashion, the blower power demand actually provides a slight buffer for the system power. This is acceptable since the fuel cell thermal response time scale

is so much larger than other system response times. In effect, the blower power is increased as fast as possible minimizing negative effects to the system power response. In the system used here, the fuel cell stack was designed to provide as much as 10% of total power to the blower (system parasitic loads). Hence saturation (Sat) is used such that the blower power will not ever demand more than 10% of the system power demand, as shown in Fig. 3.

In addition to the fuel cell temperature, the fuel cell inlet air temperature must also be controlled to avoid large thermal gradients in the fuel cell. To control the cathode inlet air in the current system, the amount of air bypassing the high temperature heat exchangers is manipulated. This can be accomplished by a simple feed-forward and feedback controller. Since the time scale for manipulation of the control valves is significantly faster than the thermal response time of the system, this type of control is straightforward with heat exchangers that are sufficiently sized.

To help clarify input and output pairing and the control structure the overall integrated baseline controller is presented in Fig. 4. In summary, the controller is composed of five primary components, a blower cascade controller to control the fuel cell stack temperature by manipulating the blower shaft speed my demanding the fuel cell to generate more or less power for the blower, a blower power saturation such that the blower power evaluated to be the difference between the system (external) power demand and the fuel cell power is always equal or greater than zero, a fuel cell power controller to manipulate the current such that the fuel cell meets both the system external power demand and the blower power demand without depleting all the fuel within the fuel cell, a fuel flow controller to operate the fuel cell at constant fuel utilization, and a cathode inlet temperature controller to control the cathode inlet air temperature.

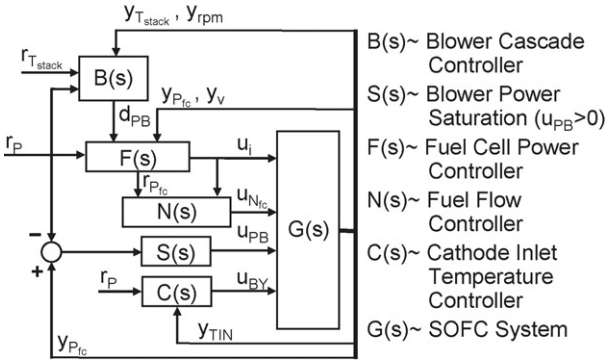

Fig. 4. Integrated base line controller (*y* indicates system feedback value, *r* indicates reference set point value, *u* indicates system input value, *d* indicates demand value).

4.3. Simulation results

Results from simulation of the baseline controller implemented into the integrated dynamic model of the system are presented in Fig. 1. An instantaneous system load demand increase from 2 to 5 kW, occurring at time $t = 0$, was simulated. The system power, voltage, and current response are shown in the uppermost plot of Fig. 5.

With the rapid current response caused by the combination of feed-forward and feedback control with large gains the system power was able to follow the load demand for approximately a third of a second (Fig. 5). Hydrogen stored within the volume of

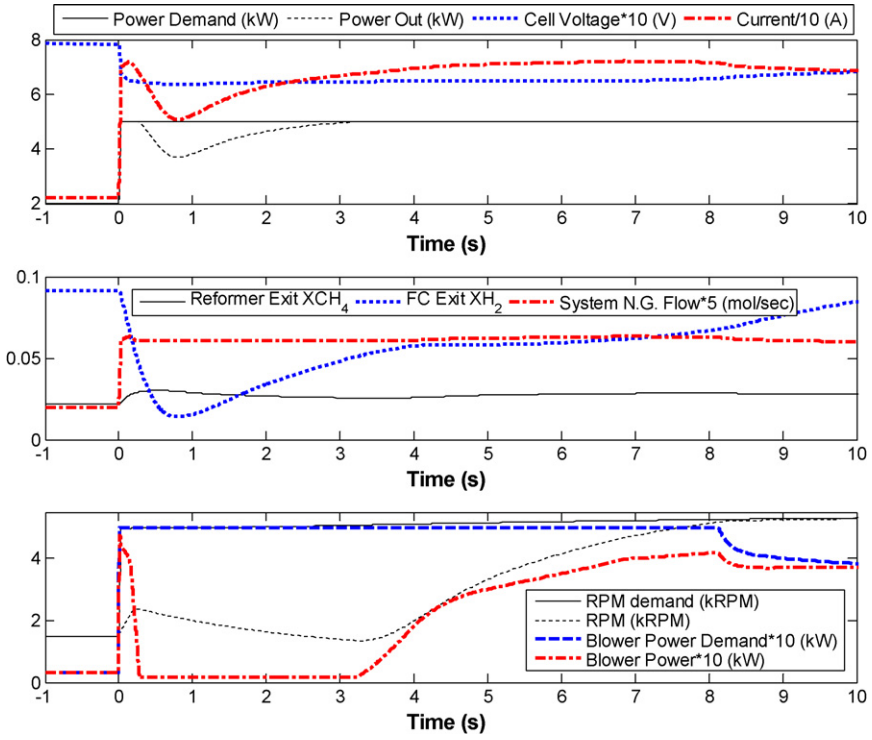

Fig. 5. Short time response to a simulated 2–5 kW load increase with the baseline controllers implemented.

the fuel cell compartment provides a slight capacitance such that the power demand could be initially tracked. After a fraction of a second the hydrogen within the fuel cell anode compartment started to become depleted causing the fuel cell voltage to drop below the minimum 0.65 cell voltage criterion used in the power reference governor. Because of this low fuel cell voltage condition, the reference governor loweres the system power demand to avoid hydrogen depletion in the fuel cell and to maintain a minimum fuel cell voltage. From the middle plot of Fig. 5 it can be seen that the fuel cell anode exit mole fraction (X_{H_2}) did not reach zero. However, if the power demand had not been lowered, the hydrogen would have become depleted, the fuel cell voltage would have plunged, and the fuel cell anode would begin to oxidize.

With the reference governor, the system power was reduced, and the hydrogen within the fuel cell was not depleted. As more fuel was supplied to the fuel cell following the saturation, the fuel cell hydrogen mole fraction increased. The natural gas fuel flow to the system increased almost instantaneously because of the feed-forward action of the controllers. The flow from the reformer to the fuel cell was delayed by both from the chemical kinetics and mass flow dynamics in the reformer. Once sufficient hydrogen reached the fuel cell anode compartment the system power was tracked. It is important to note that the reformer energy conservation, heat transfer and chemical kinetics have been captured in the model. The reformer system simulated includes thermal management to assure that sufficient methane conversion is sustained during the transient. At low power the reformer exit reformate temperature is 964 K. A few seconds following the transient the reformer reformate temperature drops to 950 K due to increased endothermic cooling followed by a longer-term transient that stabilizes at a steady state temperature of 907 K for high power conditions. The reformate temperature changes with operating power, but the reformer temperature is maintained at levels sufficient for methane chemical conversion. With decreased reformer temperature the resulting methane concentrations at the reformer exit increase. The high reformer temperature in the present system is a result of the reformer integration with fuel cell exhaust through two heat exchangers and is not a coincidence. With temperature thus maintained, the reformer residence time is designed to be longer than the chemical kinetics required ensuring sufficient methane conversion.

The blower was used to provide some buffer for the system power. The blower shaft speed demand set point, the actual blower shaft speed, the blower power demand set point, and the actual blower power are plotted in the third plot of Fig. 5. Following the load increase the blower shaft speed demand set point and the blower power demand set point increased instantaneously due to the feed-forward portion of the blower controller. The actual blower power increases initially but becomes zero when the hydrogen became depleted in the fuel cell. This provided a slight buffer for the system power response. The blower power is later allowed to increase once the system power set point was met. The blower shaft speed then increased to the demanded shaft speed in approximately 5 s.

In the baseline control simulation the system power reference governor was actuated to limit the current to avoid hydrogen depletion in the fuel cell anode compartment to account for the reformer flow delay. As soon as the fuel flow reached the fuel cell, the system power could be tracked exactly. Overall, the system power was able to track the instantaneous power demand increase from 2 to 5 kW within about 3 s.

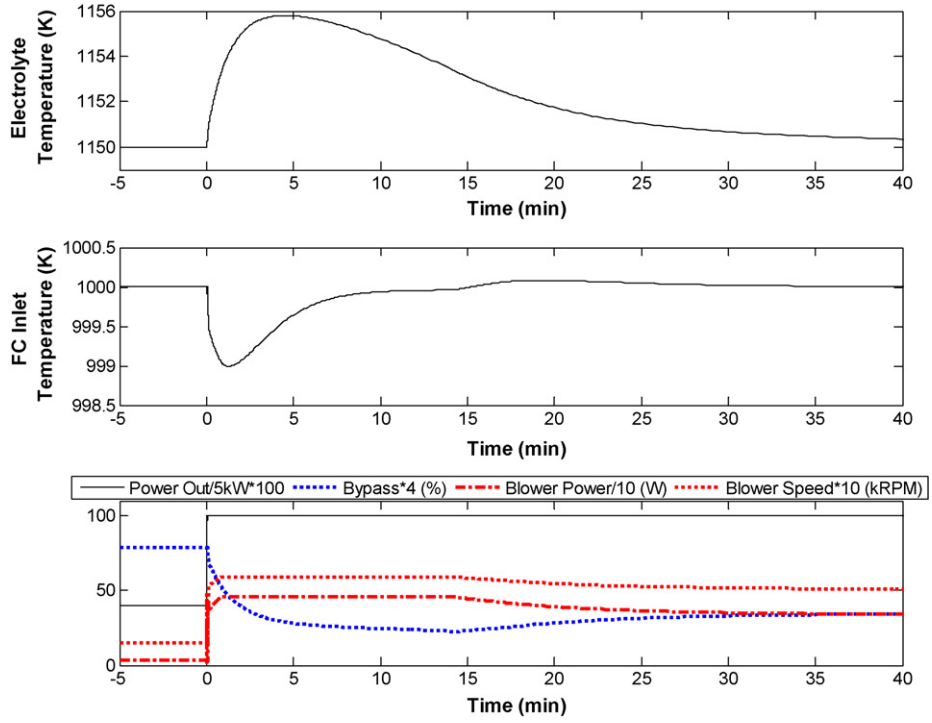

Fig. 6. Thermal response to a simulated 2–5 kW load increase with the baseline controllers implemented.

As shown in Fig. 6 the magnitude of the temperature rise was less than 10 K. The fuel cell electrolyte temperature response remained within operating requirement. This is because the blower response is much faster than the thermal response of the fuel cell. The blower air flow can effectively be controlled to maintain the fuel cell temperature sufficiently; although the precipitous temporary drop in blower RPM required by the current power controller might be undesirable. The cathode inlet temperature (Fig. 6) was controlled to within a degree of the set point temperature by manipulating the heat exchanger bypass valve. This simulation demonstrates that if only the fuel cell thermal response is considered, an SOFC system can rapidly follow significant dynamic variations in power demand in the time it takes for fuel flow manipulations to reach the fuel cell anode compartment (to avoid hydrogen depletion). The fuel cell inlet temperature and electrolyte temperature can be controlled without affecting the system load following capability.

With sufficient attention to controller and fuel cell system design, the above results establish that control of fuel cell temperature does not limit SOFC transient load following capability. On the other hand, the response of the combustor temperature for the previous simulation may be of some concern. The combustor temperature response is shown in Fig. 7. Within ten seconds of the power demand increase the combustor exit temperature fluctuated close to 100 K. Initially, the combustor temperature decreases slightly because more fuel is consumed in the fuel cell immediately following the load change and before the fuel flow rate can be increased. This results in less fuel being sent to the combustor, lowering the combustor temperature initially. After the additional fuel enters and exits the fuel cell (at essentially constant utilization) the combustor temperature significantly increases as shown in Fig. 7. The increase in temperature is caused because the combustor fuel flow increases before the combustor air flow increases, which leads to a temporary increase in the combustor fuel to air ratio.

The baseline control design produces a SOFC system with very effective dynamic load following capability. This capability is fundamentally limited by depletion of hydrogen (electrochemically active species) in the anode compartment caused by fuel flow delays in the system. The simulation indicates that thermal gradients in the combustor are also a case of concern. In the baseline controller design the combustor temperature could in part be controlled by manipulating the air flow rate more quickly. However in this case the blower parasitic power would affect the system power output response. In the current strategy, a tradeoff must be made, either the combustor temperature is not controlled tightly, or more blower power is utilized to mitigate combustor temperature transients at the expense of tracking the system power. The two problems with the baseline controller thus are hydrogen depletion and the combustor temperature blower parasitic power tradeoff.

These two problems are actually coupled. It could be possible to send more fuel through the system to avoid hydrogen depletion, essentially flooding the fuel cell, but this would result in high combustor temperatures. Hence, with this control structure it is challenging to further improve and optimize load following because of the coupling between (1) hydrogen depletion, (2) the combustor temperature, and (3) parasitic power losses. An alternative control strategy and system control structure may be able to control combustor temperature, while at the same time improve system dynamic load following capability. Such a control structure will be aimed at resolving the tradeoff between the combustor temperature and blower power. However, hydrogen depletion will remain a fundamental limitation to SOFC system load following capability.

5. Improved control strategy and design

5.1. Fuel cell current combustor temperature controller

In the baseline controller, it is difficult to control the combustor temperature, because the air flow rate cannot increase as fast as the fuel flow rate without affecting the system power. The new control approach is to manipulate the fuel cell current to control the combustor inlet stoichiometry. In order to limit the impact of the blower power demand on load following, varying the fuel cell current will vary the amount of hydrogen consumed, which will affect the amount

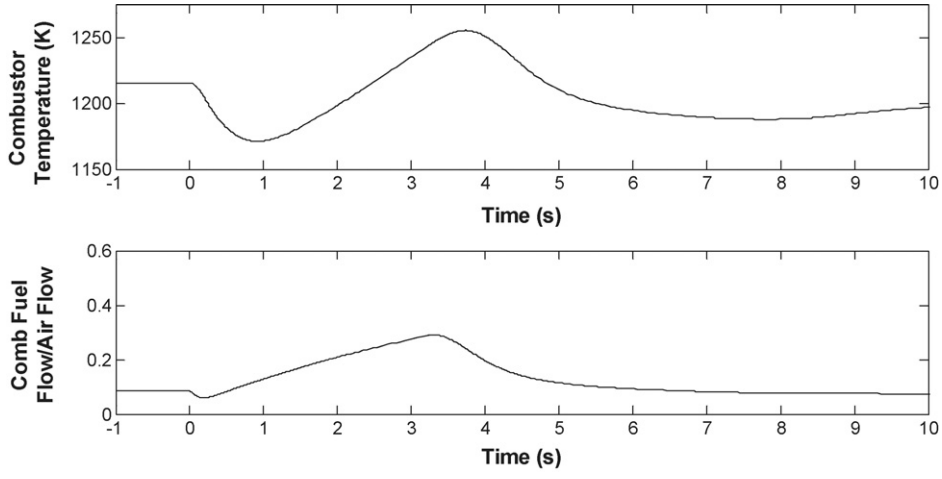

Fig. 7. Combustor temperature, and combustor fuel flow and air flow ratio response to a simulated 2–5 kW load increase with the baseline controllers implemented.

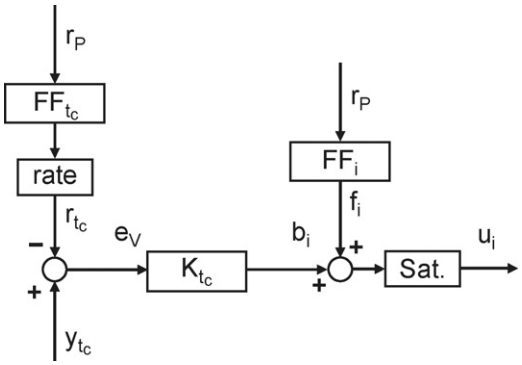

Fig. 8. Fuel cell current combustor temperature controller (*y* indicates system feedback value, *r* indicates reference set point value, *e* indicates error between feedback and set point value, *g* indicates modified/governor contribution, *u* indicates system input value, *f* indicates feed-forward contribution, *b* indicates feedback contribution, *d* indicates demand value).

of hydrogen entering the combustor and thus the combustor temperature.

This can be accomplished by a simple fuel cell current feedback controller on the combustor temperature as shown in Fig. 8.

Increasing the SOFC current to decrease the combustor fuel content to control temperature will result in increased fuel cell power. This is beneficial because the increased fuel cell power is sent to the blower thereby increasing the air flow rate. The increase in fuel cell power also results in increased heat generation within the fuel cell. In essence, the new control strategy is transporting the transient combustor temperature problem to the fuel cell in the form of additional heat generation within the fuel cell while the air flow rate is still increasing. Shifting the extra heat from the combustor to the fuel cell is possible through the manipulation of the fuel cell current. The current has a faster response time than the combustor temperature response due to transport delays through the reformer and fuel cell. This shift is advantageous because the additional heat generation within the fuel cell can be safely managed since the thermal capacitance of the fuel cell is large, and extra power generated will allow the blower to counter the heat.

The new control strategy manipulates the SOFC fuel utilization during transients to maintain the combustor temperature. Controlling the combustor temperature in this manner can also be considered an alternative control strategy for avoiding fuel depletion in the fuel cell, similar to the voltage governor presented in Fig. 2. In the decentralized control case, it is only possible to directly control as many outputs as manipulated inputs. In this new proposed control structure explicit control of fuel utilization is replaced by explicit control of the combustor temperature. However by controlling the combustor temperature, safe limit on fuel utilization is maintained. The fuel cell outlet or combustor inlet fuel content is the main variable that affects the combustor temperature, together with the air flow rate. The combustor temperature is rapidly affected by decreasing fuel content (i.e. depleting SOFC exit fuel content) such that current will not deplete fuel in the fuel cell to maintain the combustor temperature.

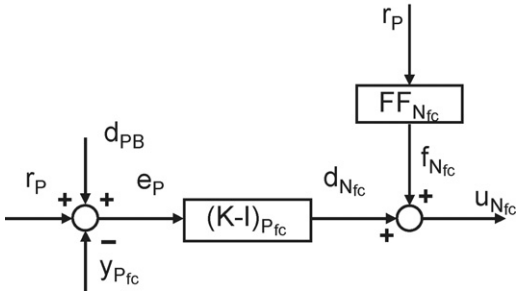

Fig. 9. Fuel flow fuel cell power controller (*y* indicates system feedback value, *r* indicates reference set point value, *e* indicates error between feedback and set point value, *g* indicates modified/governor contribution, *u* indicates system input value, *f* indicates feed-forward contribution, *b* indicates feedback contribution, *d* indicates demand value).

Even though it is desired to manipulate utilization during transients, it is desired to maintain constant fuel utilization at steady state. To maintain constant utilization at steady state, the combustor temperature set point (r_{t_c}) is varied. Note that the respective combustor temperature set points where determined from steady state operation of the baseline control system. The fuel cell current-combustor temperature controller is illustrated in Fig. 8. Constants used in the controller are presented in Table 2.

With the fuel cell current essentially used to control the combustor temperature, the system power is varied by manipulating the fuel flow rate, and the system power is not controlled directly by the fuel cell current. Instead, the fuel cell power ($y_{P_{fc}}$), equal to the external power demand (r_p) plus blower power demand (d_{PB}) is controlled (see Fig. 9) by manipulating the fuel flow rate ($u_{N_{fc}}$).

Controlling the fuel cell power through fuel flow is more sluggish than control by manipulating the current. Following a transient or disturbance the fuel cell power will not be tracked exactly. However, the tracking error will first affect the blower then the system power output. Recall that the blower power is used as a buffer on the system power output, thus small errors in fuel cell power tracking will not affect the ability of the system to track power demands. Since the fuel cell thermal capacitance is large, temporary offsets between the blower power demand and actual blower power is acceptable, particularly since excess power, once the fuel enters the fuel cell, can be used to ramp up the blower. Integral feedback is used to ensure zero steady state tracking.

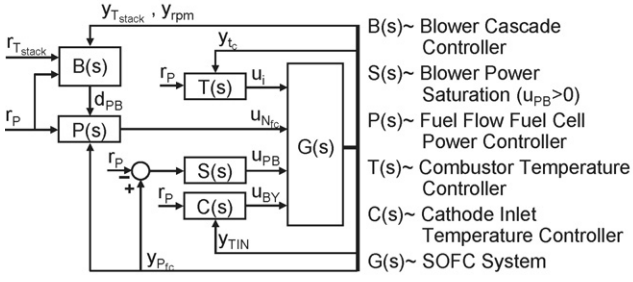

Fig. 10. Integrated novel controller (*y* indicates system feedback value, *r* indicates reference set point value, *u* indicates system input value, *d* indicates demand value).

The reformer flow delay is a fundamental limitation to transient load following. The new integrated control strategy (demonstrated in Fig. 10) contains an external loop where fuel is manipulated to control power. To avoid oscillation caused by the fuel delay, feedback gain in the external loop cannot be too large. The other control loops in the system are faster inner loops which maintain the system operating condition. This structure is effective because the faster inner loops can reject disturbances and transients caused by the delay limited external loops. Even though the inner loops are inherently more responsive than the external loop, careful consideration (through simulation in this case) must be taken in designing feedback gains to avoid instabilities due to coupling. For example, the effects of fuel flow and current are coupled to both the fuel cell power and combustor temperature, and to avoid instabilities due to coupling the gains cannot be made too high. Feedback gains used in this controller are presented in Table 2.

5.2. Simulation results

To compare the load following capability of the alternative control design to the baseline design, an instantaneous system load demand increase from 2 to 5 kW was simulated with the new controllers implemented in the system. The short-time response is presented in Fig. 11. Initially the fuel cell power rapidly increased due to feed-forward actuation of the current based on the power demand. In this time the system power was tracked and the increased fuel cell power was absorbed as in increase in the blower power. Shortly after the combustor temperature decreased because of increased electrochemical reactions in the fuel cell without an increase in fuel flow. Due to the combustor temperature feedback the current was decreased such that more fuel could be reacted in the combustor instead of the fuel cell maintaining the combustor temperature. Since the fuel cell current was decreased (in control of the combustor temperature) the overall fuel cell power decreased, causing an initial decrease in blower power and secondary decrease in the system power output. As more fuel reached the fuel cell and the combustor the fuel cell voltage and current increased, such that the instantaneous load power demand was tracked within approximately a second and a half.

Similar to the baseline, the system cannot track power exactly because of the reformer flow delay causing the fuel to become depleted in the fuel cell. Nonetheless, the system power response tracked demand better using the novel alternative controller. Since the fuel flow is directly manipulated to control the fuel

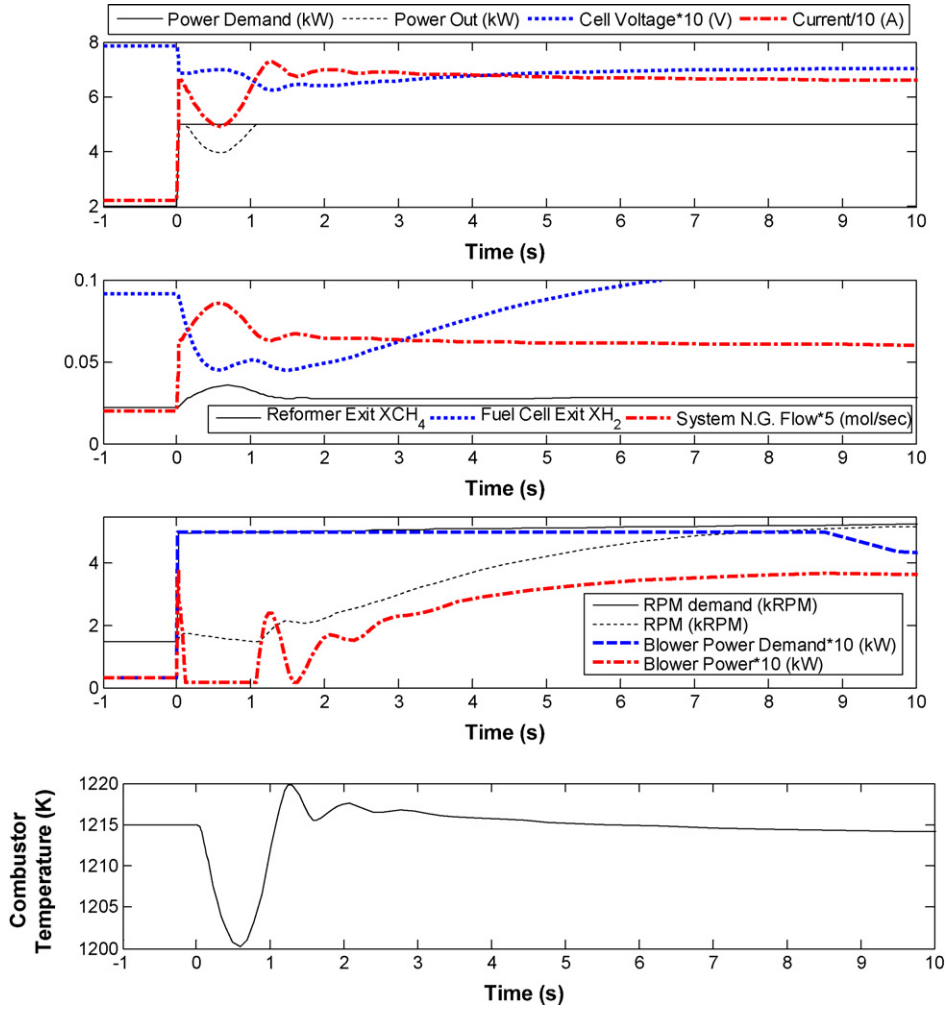

Fig. 11. Short time response to a simulated 2–5 kW load increase with the novel controllers implemented.

cell power, more fuel was sent through the reformer during the time period when the power was limited due to hydrogen depletion in the fuel cell. This helped to more quickly increase the fuel flow to the fuel cell up to the level required for the increased load power demand.

Manipulating the current to control the combustor temperature was effective. From Fig. 11, it can be seen that the combustor remained within approximately 10° of the set point value. Once the fuel flow rate increased, and before the air flow rate can be increased, the combustor temperature rises. However, in this case the combustor temperature rise was less severe, because manipulation of the fuel cell current effectively controlled the fuel-to-air ratio in the combustor by lowering the inlet fuel flow. Note also that the current is able to control the combustor temperature without saturating.

Dynamics in the fuel cell power from manipulating current to control the combustor temperature are absorbed by the blower. It can be seen from Fig. 11 that the actual blower power does not track the blower power demand initially. The power fuel flow feedback gain cannot be too large if instabilities are to be avoided, therefore, the feedback cannot make up for all of the tracking error during the transient. However, a mismatch between the actual blower power and blower power demand set point is acceptable from a system operating requirement standpoint. Simulation indicates that the fuel cell temperature remained within approximately 10° of the set point value.

Following the slight mismatch between system power and power demand caused by hydrogen depletion, the power demand was tracked (Fig. 12). The combustor temperature was maintained within 20° of the set point during the entire period of the simulation, including during the time when the set point temperature was lowered to raise the fuel utilization. This demonstrates that the current can be effectively manipulated to control the combustor temperature. For most of the power transient the system efficiency remained above 50%. Manipulating the combustor temperature set point allowed for the steady state fuel utilization to be approximately 85%, even though the fuel utilization varied during the transient.

The blower power is used as a buffer to improve load following. This may be of some concern since the blower is used to control the fuel cell temperature, and control of the fuel cell temperature is crucial to fuel cell stack robustness and life. However, simulation results shown in Fig. 13 indicate that with the improved control strategy the fuel cell temperature can be effectively controlled to within 10° for this very significant 150% load power demand increase (2–5 kW). Slight variations in the blower power, caused by transients in the fuel cell did not significantly affect the fuel cell thermal response because the heat capacity and thermal time response of the fuel cell are large. Simulation further indicates that the controlled cathode inlet temperature response is also well maintained during the transient. Therefore, it appears that the fuel cell thermal response is sufficiently controlled for the current significant, instantaneous increase in power. Overall it has been demonstrated that the alternative controller can load follow within hydrogen depletion constraints, while maintaining system parameters within operating requirements. An overview of how each operating requirement is addressed in the alternative controller in the specific system is provided below.

(1) Water is supplied externally to the system in proportion to the fuel flow rate to ensure sufficient steam-to-carbon ratio in the reformer and anode compartment.
(2) To maintain the combustor temperature hydrogen cannot be depleted in the fuel cell anode compartment. The fuel cell current is manipulated to control the combustor temperature.
(3a) The system heat exchangers are designed such that fuel cell heat is provided to the inlet air to raise the air temperature to within 200° of the fuel cell operating temperature. The cathode inlet temperature can be closely controlled by bypassing air around the heat exchangers.
(3b) An external steam reformer is incorporated within the system. The system configuration is designed (a) such that the reformer operating temperature is sufficiently high and (b) with a residence time longer than the kinetics time such that high methane-to-hydrogen conversion can be achieved.

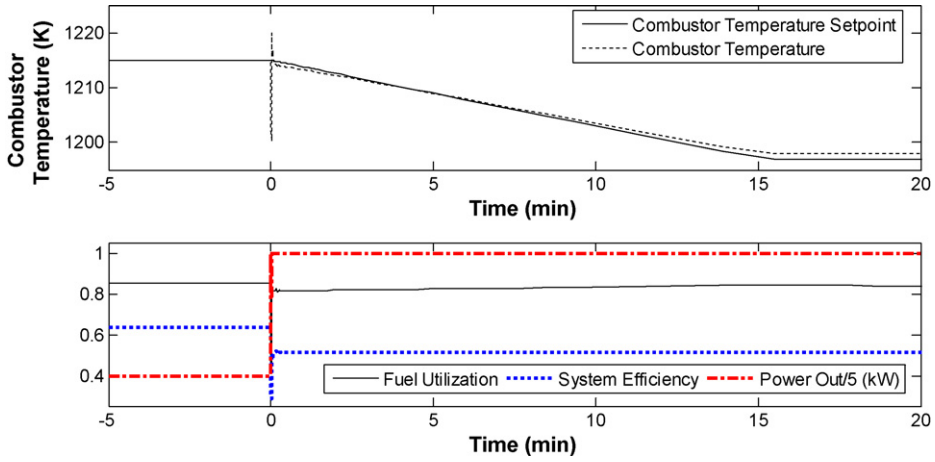

Fig. 12. Combustor temperature, fuel utilization, system efficiency, and system power response to a simulated 2–5 kW load increase with the novel controllers implemented.

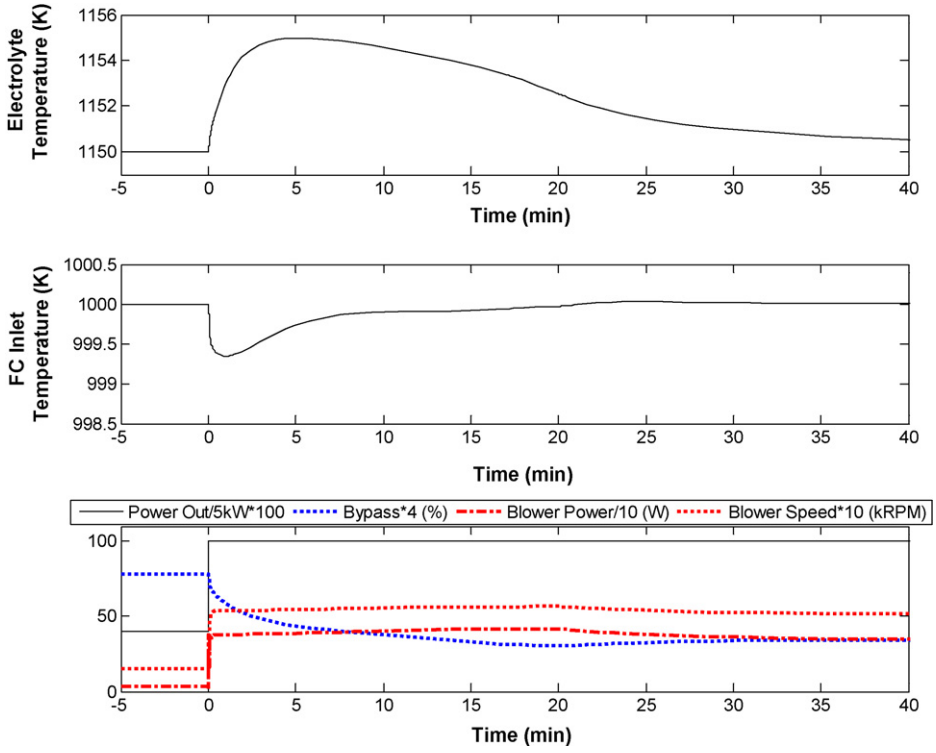

Fig. 13. Fuel cell thermal response to a simulated 2–5 kW load increase with the novel controllers implemented.

(3c) The current is manipulated to control the combustor temperature and heat exchanger temperatures can be sufficiently maintained.
(4a) A variable speed blower is used, to manipulate the air flow to control the fuel cell temperature to within 10° during transients and to within a few degrees at steady state.
(4b) By maintaining sufficient electrochemically active species in the fuel cell anode compartment, the voltage is maintained above a minimum value.

It has been demonstrated that load following in the simulated system is limited by the amount of electrochemically active species (hydrogen) available within the fuel cell anode compartment. Therefore, it appears that SOFC systems can be designed to load follow exactly with the strict limitation of hydrogen depletion. The extent in which a particular fuel cell system design can load follow depends in how fast hydrogen can be provided to the fuel cell anode, upon the amount of hydrogen that is "stored" within the fuel cell anode compartment, and upon the operating conditions before and after a load transient.

6. Discussion

From the perspective of mass, momentum, and mass conservation, and the operating requirements and simulation results presented herein, it appears that SOFC systems can be designed to have significant load following capabilities. Conducted simulations reinforce the fact that even though SOFC systems are nonlinear coupled systems, decentralized linear controls can be effectively utilized to control properly designed integrated SOFC systems. A fundamental limitation to SOFC system load following capability is hydrogen depletion in the fuel cell anode compartment. The innovative control strategy was more effective at mitigating reformer flow delay affects on the system than the baseline controller. A perfect load following SOFC system could not be produced in the current effort. Potential system design solutions that could address the fundamental limitation of SOFC system load following caused by hydrogen depletion include:

(1) The power that cannot be met through the fuel cell can be provided by an external source. For example the grid could be used to "make up" the power that the fuel cell itself cannot provide.
(2) Energy storage such as through batteries, capacitors, and flywheels could be used to meet the power demand that cannot be met by the fuel cell during transients.
(3) Systems could be designed to have improved load following at the cost of efficiency, such as by lowering the steady-state fuel utilization. This would results in essentially storing energy within the fuel cell anode compartment to avoid hydrogen depletion limitations. Advanced control strategies, may be able to use this fact to vary utilization depending on the time of day to improve load following capability when transient load increases can be predicted. It may also be possible to "flood" the reformer during a load transient such that the fuel flow to the fuel cell would increase and allow for quicker load following. However, the amount of current drawn from the fuel cell is limited and therefore the extent to which the reformer can be "flooded" is also limited by the need to control the combustor temperature.

(4) More effective cycle configurations, system components and more advanced controls can be developed to improve the system load following. For the current SOFC system, load following was limited by the reformer flow delay and the amount of hydrogen stored in the fuel cell. If the reformer did not have such a flow delay, hydrogen could be supplied to the fuel cell anode compartment more rapidly to avoid hydrogen depletion. Development of pure internal reforming systems, where the fuel enters the fuel cell directly could also significantly improve load following since these systems would have essential no fuel flow delay. This may, however, come at the expense of increased thermal gradients in the cell.

Each of these potential control solutions for advancing SOFC load following capability has a different cost associated with its use. Determining the lowest cost option for the design of any particular level of load following capability is not trivial, and depends upon the performance requirements of the system, and the dynamic nature of the load. The challenge of hydrogen depletion has been identified as a fundamental limitation to SOFC system load following capability that has not been resolved herein.

7. Summary

Dynamic modeling has been used to design and evaluate controls for advancing load following capability in SOFC systems. Fuel cells inherently have rapid load following characteristics, however, the load following capability of practical SOFC systems must be limited to maintain the SOFC system parameters within operating requirements. Dynamic modeling provides an effective means to investigate controls without risking loss or deterioration of expensive SOFC systems. Using the a first principles integrated dynamic model of a SOFC system it has been shown that fuel cell anode compartment hydrogen depletion fundamentally limits load following capability. Controlling the fuel cell electrolyte temperature, the fuel cell inlet temperatures, and combustor temperature are not limiting challenges as demonstrated by dynamic system simulations in which a novel alternative controller was used. The fuel cell stack temperature can be controlled by manipulating the airflow, the anode and cathode inlet temperatures can be well maintained by properly sizing system heat exchangers and bypassing air, and the combustor temperature can be controlled by manipulating the fuel cell current.

Three innovative control concepts have been investigated:

1. The fuel cell current can be manipulated to control the combustor temperature. Essentially the current can manipulate the fuel flow to the combustor to control the combustor temperature.
2. The air blower power can be used to buffer the system power response without affecting the fuel cell thermal response.
3. A variable speed blower control strategy can be utilized to maintain the fuel cell temperature. This control technique is shown to be very practical.

8. Conclusions

From the simulation results with the developed controllers implemented, it seems reasonable that SOFC systems should be able to load follow in the time required for changes in fuel flow to reach the anode compartment. A control structure has been designed to mitigate the effects of hydrogen depletion but some means of energy storage will be needed to resolve the problem in practical systems if ideal load following is to be achieved. Nonetheless, it has been shown that future SOFC systems with proper system and control design should have superior load following capabilities. It will take time for SOFC system manufactures to gain confidence in their systems and controls. However, major improvements in SOFC load following capability are possible, and the rapid load following capability of SOFC systems could become a major competitive advantage, which would further motivate the advancement of SOFC systems.

Appendix A. Summary of dynamic system model

Each of the six primary system components (SOFC, steam reformer, steam preparation boiler, oxidizer, heat exchangers, and blower) are modeled individually and integrated to form the system. The flow between each of the components is resolved for molar flow rate, species concentration (CH_4, CO, CO_2, H_2, H_2O, N_2, O_2), temperature and pressure. To resolve the molar flow rate, species concentration, temperatures and pressure, a control volume conservation analysis is conducted in each component using the well stirred assumption.

A.1. Heat exchangers and steam preparation boiler

Heat exchangers in the model are modeled as presented in [3,6,8]. Each heat exchanger is discretized into hot and cold streams and the plate separating the two streams. The three control volumes are then used to discretize the heat exchanger into five nodes in the stream-wise direction. The temperature and species mole fractions in gas control volumes of the heat exchanger, as well as the combustor and fuel cell model, are determined from solution of the dynamic energy and species conservation equations in the general form:

$$NC_V \frac{dT}{dt} = \dot{N}_{in} h_{in} - \dot{N}_{out} h_{out} + \sum \dot{Q}_{in} - \sum \dot{W}_{out} \quad (A1)$$

$$N \frac{dX_i}{dt} = \dot{N}_{in} X_{i,in} - \dot{N}_{out} X_{i,out} + \dot{R}_i \quad (A2)$$

where the exit molar flow rate is found from:

$$\dot{N}_{out} = \dot{N}_{in} + \sum \dot{R}_i \quad (A3)$$

The temperature of solid control volumes is found from solving the dynamic solid-state energy conservation equation in the general form:

$$\rho V C \frac{dT}{dt} = \sum \dot{Q}_{in} - \sum \dot{W}_{out_i} \quad (A4)$$

Convection heat transfer between each stream and the plate is modeled using Newton's law of cooling, and Fourier's law is used to model conduction heat transfer along the heat exchanger plate. The steam reformation boiler is essentially a heat exchanger between the fuel and steam mixture and the fuel cell exhaust where the latent heat of water evaporation is captured in the first node of the heat exchanger.

A.2. Combustor

The combustor is modeled as a single control volume as presented in [5,6,8]. The combustor contains two inlet streams (i.e., anode exhaust, and cathode exhaust) and a single exhaust stream. To simplify the model, the combustor is assumed to operate adiabatically with complete fuel oxidation. Then the exit mole fractions can be determined from Eq. (A2) and the outlet temperature from Eq. (A1). The thermal capacitance associated with the mass of combustor and catalyst is included in the energy conservation equation.

A.3. SOFC

Each cell unit in the stack, i.e., cathode gas, cathode, electrolyte, anode, anode gas, and separator plates (interconnects) are assumed to operate identically, such that simulation of a single cell unit is taken as representative of the entire stack performance. The cathode gas, electrode–electrolyte assembly, anode gas, and separator plate each represent a single bulk control volume of the fuel cell model. Convection heat transfer is modeled between each gas and solid control volume (e.g., cathode gas and electrode–electrolyte assembly; anode gas and electrode–electrolyte assembly; anode gas and separator plate). Note that radiation heat transfer between the electrode–electrolyte assembly and the separator plate is neglected because in the planar, co-flow, intermediate temperature fuel cell design, heat exchange is dominated by convection.

Temperatures and species mole fractions in the anode and cathode gas streams are determined from dynamic Eqs. (A1)–(A3). Eq. (A4) is used to determine temperatures in the anode electrode plate, and electrolyte. To avoid algebraic equilibrium constraints, steam reformation chemical kinetics from [20,21] are based on the exit flow conditions are used in the anode control volume as was done in [3,5,6,8]. Electrochemical reaction rates in the SOFC are determined from the current, an input to the fuel cell model, based on Faraday's law and SOFC half reactions.

The fuel cell exit flow is evaluated from the orifice flow equation:

$$\dot{N}_{\text{out}} = \dot{N}_{\text{o}}\sqrt{\frac{P_{\text{in}} - P_{\text{out}}}{\Delta P_{\text{o}}}} \tag{A5}$$

where P_{out} is atmospheric pressure and P_{in} is the fuel cell pressure evaluated as:

$$\frac{\mathrm{d}P}{\mathrm{d}t} = \frac{RT}{V}(\dot{N}_{\text{in}} - \dot{N}_{\text{out}} + \sum \dot{R}_i) \tag{A6}$$

Since the electrochemistry and power electronic time scales are very fast, it is assumed that the current changes instantaneously in the fuel cell. The corresponding voltage is determined quasi-steadily using time variant fuel cell exit temperatures, and species mole fractions. The electrochemical voltage model presented in [3,5,8], is used to account for Gibbs free energy, activation polarization, and concentration polarization. The Ohmic polarization model is adapted from [29] to capture temperature effects on the Ohmic resistance.

A.4. Steam reformer

The steam reformer model was adopted from [5,8]. The heat required for steam reformation is supplied by the system's exhaust. To capture reformation kinetics and heat transfer the reformer is discretized using three control volumes, the reformer channel, a separator wall, and the exhaust stream. The three control volumes are then used to discretize the reformer into five control volumes along the stream wise direction. The reformer was discretized in the flow direction because of the importance of heat transfer between the exhaust and the reformate stream. The temperatures and species mole fractions in the reformer model are determined from Eqs. (A1)–(A4). As was accomplished in the fuel cell model, the chemical reaction rates are determined based on each nodes exit conditions. Convection heat transfer between the exhaust and the reformer separator wall, and between the separator wall and the reformate stream is resolved. Fourier's law is further used to capture heat transfer along the separator wall. A reformer flow delay was evaluated at the reformate exit. The pressure within the reformer is evaluated from:

$$\frac{\mathrm{d}P}{\mathrm{d}t} = \frac{RT}{V}(\dot{N}_{\text{in}} - \dot{N}_{\text{out}} + \sum \dot{R}_i) \tag{A7}$$

From which the reformer exit flow can be determined from

$$\dot{N}_{\text{out}} = \dot{N}_{\text{o}}\sqrt{\frac{P_{\text{in}} - P_{\text{out}}}{\Delta P_{\text{o}}}} \tag{A8}$$

where P_{in} is the reformer pressure and P_{out} is the fuel cell pressure. This simulates a first order fuel flow delay to the fuel cell.

A.5. Blower

The variable speed blower model represents the variable frequency drive (VFD) blower motor and blower blades of the system. The governing equation of the blower is the state space representation of the blower rotational velocity obtained from a dynamic shaft torque balance:

$$\text{Jw}\frac{\mathrm{d}w}{\mathrm{d}t} = (\dot{W}_{\text{motor}} - \dot{W}_{\text{thermo}})1000 \tag{A9}$$

where the blowers thermodynamic work is evaluated from:

$$\dot{W}_{\text{thermo}} = \frac{1}{\eta}\frac{\gamma RT_{\text{amb}}}{\gamma - 1}\left[\left(\frac{P_{\text{out}}}{P_{\text{amb}}}\right)^{\gamma - 1/\gamma} - 1\right] \tag{A10}$$

With the blower efficiency assumed to be 85%. The compressor outlet pressure and outlet flow rate are modeled to be linearly proportional to the blower shaft speed

$$P_{\text{out}} = \frac{15\,(\text{kPa})}{5000\,(\text{rpm})}\text{RPM}\,(\text{rpm}) + 101.325\,(\text{kPa}) \quad \text{(A11)}$$

$$\dot{N}_{\text{out}} = \frac{0.0008\,(\text{kmol}\,\text{s}^{-1})}{5000\,(\text{rpm})}\text{RPM}\,(\text{rpm}) \quad \text{(A12)}$$

where the nominal blower shaft speed is 5000 rpm corresponding to a blower pressure of 15 kPa and a blower air flow rate of 0.0008 kmol s^{-1}. Assuming a linear relationship between the shaft velocity, flow rate, and pressure ratio in the blower is a good simple first approximation [8].

References

[1] M.R. Andrew, in: K.R. Williams (Ed.), An Introduction to Fuel Cells, Elsevier Publishing Company, New York, 1966.
[2] J. Brouwer, F. Jabbari, E.M. Leal, T. Orr, J. Power Sources 158 (1) (2006) 213–224.
[3] R. Roberts, J. Brouwer, J. Fuel Cell Sci. Technol. 3 (18) (2006) 18–25.
[4] T. Kaneko, J. Brouwer, G.S. Samuelsen, J. Power Sources 160 (1) (2006) 316–325.
[5] F. Mueller, J. Brouwer, F. Jabbari, S. Samuelsen, J. Fuel Cell Sci. Technol. 3 (2) (2006) 144–155.
[6] F. Mueller, F. Jabbari, J. Brouwer, R. Roberts, T. Junker, H. Ghezel-Ayagh, Control Design for A Bottoming Solid Oxide Fuel Cell Gas Turbine Hybrid System, ASME, Irvine, CA, 2006.
[7] R. Roberts, J. Brouwer, F. Jabbari, T. Junker, H. Ghezel-Ayagh, J. Power Sources 161 (2006) 484–491.
[8] F. Mueller, Design and Simulation of A Tubular Solid Oxide Fuel Cell System Control Strategy, Masters, University of California, Irvine, 2005, p. 141.
[9] R. Roberts, A Dynamic Fuel Cell-Gas Turbine Hybrid Simulation Methodolgy to Establish Control Strategies and an Improved Balance of Plant, Dissertation, University of California, Irvine, 2005, p. 338.
[10] C. Stiller, B. Thorud, O. Bolland, R. Kandepu, L. Imsland, J. Power Sources 158 (1) (2006) 303–315.
[11] M.L. Ferrari, L. Magistri, A. Traverso, A.F. S Massardo, Proceedings of the Control System for Solid Oxide Fuel Cell Hybrid Systems, ASME, Reno-Tahoe, Nevada, USA, June 6–9, 2005, pp. 1–9.
[12] M.L. Ferrari, A. Traverso, L. Magistri, A.F. Massardo, J. Power Sources 149 (2005) 22–32.
[13] R. Kandepu, L. Imsland, B.A. Foss, C. Stiller, B. Thorud, O. Bolland, Energy 32 (2007) 406–417.
[14] Y. Inui, N. Ito, T. Nakajima, A. Urata, Energy Conversion Manage. 47 (15–16) (2006) 2319–2328.
[15] A. Nakajo, C. Stiller, G. Harkegard, O. Bolland, J. Power Sources 158 (1) (2006) 287–294.
[16] A. Selimovic, M. Kemm, T. Torisson, M. Assadi, J. Power Sources 145 (2) (2005) 463–469.
[17] D. Brewer, Mater. Sci. Eng. A 261 (1–2) (1999) 284–291.
[18] D. Aquaro, M. Pieve, Appl. Thermal Eng. 27 (2–3) (2007) 389–400.
[19] Y. Zhu, K. Tomsovic, Electric Power Syst. Res. 62 (1) (2002) 1–11.
[20] G.F.F. Jianguo Xu, AIChE J. 35 (1) (1989) 88–96.
[21] G.F.F. Jianguo Xu, AIChE J. 35 (1) (1989) 97–103.
[22] P. Beckhaus, A. Heinzel, J. Mathiak, J. Roes, J. Power Sources 127 (1–2) (2004) 294–299.
[23] T.J. Pukrushpan, G.A. Stefanopoulou, P. Huei, in: J.M. Grimble, A.M. Johnson (Eds.), Control of Fuel Cell Power Systems: Principles, Modeling, Analysis, and Feedback Design, Springer, London, 2005.
[24] S.K. Hazra, S. Basu, Sens. Actuators B: Chem. 115 (1) (2006) 403–411.
[25] M. Sakthivel, W. Weppner, Sens. Actuators B: Chem. 113 (2) (2006) 998–1004.
[26] X. Lu, S. Wu, L. Wang, Z. Su, Sens. Actuators B: Chem. 107 (2) (2005) 812–817.
[27] H. Iwahara, Y. Asakura, K. Katahira, M. Tanaka, Solid State Ionics 168 (3–4) (2004) 299–310.
[28] K. Katahira, H. Matsumoto, H. Iwahara, K. Koide, T. Iwamoto, Sens. Actuators B: Chem. 73 (2–3) (2001) 130–134.
[29] J.-W. Kim, A. Virkar, K.-Z. Fung, M. Karum, S. Singhal, J. Electrochem. Soc. 146 (1) (1999) 69–78.